

REYNOLDS AVERAGED NAVIER-STOKES STUDY OF THE SUBSONIC TURBULENT FLOW AROUND AN AIRFOIL USING A NON-LINEAR MODEL

Pedro Simões Flores Viana, Luís Fernando Figueira da Silva

Department of Mechanical Engineering

Pontifícia Universidade Católica do Rio de Janeiro, Rio de Janeiro, RJ, 22453-900, BRAZIL

e-mail floresviana@yahoo.com.br, luisfer@mec.puc-rio.br

André Gama de Almeida, André Luiz Martins

Empresa Brasileira de Aeronáutica SA – EMBRAER, São José dos Campos, SP, 12227-901, BRAZIL

e-mail andre.almeida@embraer.com.br, almartins@embraer.com.br

Abstract. *The computation of the lift and drag of airfoils at high angle of attack is a crucial step on aircraft design. The exact prediction of the maximum lift coefficient, the angle of attack for which airfoil stall occurs, and of the drag, is relevant early in the design process. In the past, those parameters were obtained from wind tunnel tests exclusively. This paper describes part of the results of an on-going effort to obtain some airfoil characteristics by the use of Computational Fluid Dynamics techniques. A computational study of the flow around a classical airfoil, the NLR7301, is presented. The flow conditions considered are representative of subsonic flight, and emphasis is given on the prediction of the maximum lift coefficient. Turbulence is modeled using a non-linear cubic $k-\varepsilon$ model, which accounts for near wall low Reynolds number flows. A study of the sensitivity of the computed results on the size of the computational mesh is presented, as well as a comparison between different hybrid meshes configurations. Then, the lift and drag curves are obtained for this airfoil. The computed results for pressure, lift, drag and friction coefficients are presented and compared to experimental results, whenever those are available.*

Keywords. *Turbulent flow, computational fluid dynamics, numerical study, airfoil*

1. Introduction

The airfoil design and its corresponding CFD simulation involve different problems related to the complex flowfields. The flow around airfoils, specifically when transitional or turbulent boundary layers arise, may exhibit a large sensitivity to small variations of the freestream conditions. The accurate representation of the physical phenomena involved, such as boundary layer transition and turbulence, is crucial for a correct prediction of integral quantities, as airfoil lift and drag coefficients.

This knowledge is essential during the design phase of airplanes, since the wing design process has its base on a good airfoil design. The goal of an airfoil design varies with the application envisaged. Some airfoils are designed to produce low drag, and may ultimately be required not to generate lift at all. On the contrary, some sections may need to produce low drag while yielding a given amount of lift. In some cases, the drag is not an important issue, the maximum lift is the objective function. The section may be required to achieve this performance goal with a constraint either on thickness, or on pitching moment, or on off-design performance, or other less usual constrain. No matter which is the purpose, two-dimensional Reynolds averaged Navier-Stokes (RANS) simulations have proven to be a powerful instrument to obtain the aerodynamic coefficients and to understand the nature of the flow around a given airfoil (Vos et al., 2002). However, the requirements in terms of discretization, as well as the forecast of the boundary layer transition and turbulence modeling for accurate predictions of the maximum lift (CL_{max}) and lift-to-drag ratio (L/D) still remain to be clearly established (Vos et al., 2002; Jameson, 1996; Hirshel, 1999).

This paper presents a computational study of the flow around the NLR7301 airfoil. The flow conditions considered are representative of moderate Reynolds number subsonic flight, and emphasis is given on the prediction of the maximum lift coefficient. At this high angle of attack, near stall, flow condition, the important modeling issues are the presence of a region of boundary layer separation, the existence of a laminar separation bubble, strong adverse pressure gradient and an accentuate streamline curvature.

The computations which are analyzed in the present work are carried on with a commercial CFD code, CFD++ from Metacomp Technologies (Peroomian and Chakravarthy, 1997). The definition of a simulation strategy is driven from an engineering point of view. In particular, an exhaustive parametric exploration involving variations of all possible variables that could affect the computed results is not attempted. This strategy has been chosen on the basis of design experience, Metacomp suggestions and the relatively short time required to obtain those results, typical of industry environments. Thus, turbulence is modeled using a non-linear cubic $k-\varepsilon$ model (Palaniswamy et al., 2001; Loyau, et al. 1998), which accounts for near wall low Reynolds number flows. A study of the sensitivity of the computed results on the size of the computational mesh is presented. Then, the curves of lift and drag coefficients are obtained for this airfoil. The computed results are compared to experimental results, whenever those are available.

2. Mathematical Formulation

In this work are considered moderate Reynolds number, subsonic, turbulent flows of air around the NLR 7301 airfoil. The flowfield around this airfoil is computed for several angles of attack, ranging from zero to values for which the flow on the suction side is fully separated. In order to compute this complex situation, the Reynolds Averaged Navier-Stokes (RANS) equations are solved (Wilcox, 1993). The turbulent fluxes that arise on these equations are closed using a non-linear cubic $k-\varepsilon$ model (Palaniswamy et al., 2001; Loyau, et al. 1998). This model provides for anisotropy of the Reynolds stresses and contains low Reynolds numbers terms which allow for computations extending to the viscous sub-layer. Following the notation where the rank two Cartesian tensor are noted in bold characters (**a**, **b**, etc.),

$$\mathbf{a} = a_{ij}, \quad \mathbf{ab} = a_{ik}b_{kj}, \quad \mathbf{abc} = a_{ik}b_{kl}c_{lj}, \quad \mathbf{a}^2 = a_{ik}a_{kj}, \quad \{\mathbf{a}^2\} = a_{ik}a_{ki}, \quad \mathbf{I} = \delta_{ij},$$

one may write the cubic model in canonical form as

$$\begin{aligned} \mathbf{a} = & -2C_{\mu}^* f_{\mu} \mathbf{S} + a_1 \left(\mathbf{S}^2 - \frac{1}{3} \{\mathbf{S}^2\} \mathbf{I} \right) + a_2 \left(\mathbf{WS} - \mathbf{SW} \right) + a_3 \left(\mathbf{W}^2 - \frac{1}{3} \{\mathbf{W}^2\} \mathbf{I} \right) \\ & + (b_1 \{\mathbf{S}^2\} + (b_2 \{\mathbf{W}^2\}) \mathbf{S} + b_3 \left(\mathbf{W}^2 \mathbf{S} + \mathbf{SW}^2 - \frac{2}{3} \{\mathbf{SW}^2\} \mathbf{I} \right) + b_4 (\mathbf{WS}^2 - \mathbf{S}^2 \mathbf{W}). \end{aligned} \quad (1)$$

In this equation, the non-dimensional forms of the strain and anisotropy tensors is

$$S_{ij} = \frac{k}{2\varepsilon} \left(U_{i,j} + U_{j,i} - \frac{2}{3} U_{k,k} \delta_{ij} \right), \quad (2)$$

$$a_{ij} = \frac{\tilde{u}_i \tilde{u}_j}{k} - \frac{2}{3} \delta_{ij}. \quad (3)$$

Low Reynolds number damping terms are given in Table 1. In this table, the following coefficients are used (Shih et al., 1993; Lien and Leschziner, 1996)

$$C_{\mu}^* = \frac{2/3}{1.25 + S + 0.9\Omega}, \quad (4)$$

$$S = \sqrt{2S_{ij}S_{ij}}, \quad \Omega = \sqrt{2W_{ij}W_{ij}}, \quad (5)$$

$$f_{\mu} = \frac{1 - e^{-A_{\mu}R_t}}{1 - e^{-\sqrt{R_t}}} \max\{1, (2/R_t)^{1/2}\}, \quad (6)$$

where $R_t \equiv k^2/(\nu\varepsilon)$ is the turbulent Reynolds number. This model allows for the closure of the Reynolds fluxes. One must still provide the turbulent kinetic energy and its dissipation in order to close the above equations. This is achieved by the use of a $k-\varepsilon$ model

$$\frac{\partial(\rho k)}{\partial t} + \frac{\partial}{\partial x_j} (U_j \rho k) = \frac{\partial}{\partial x_j} \left[\left(\mu + \frac{\mu_t}{\sigma_k} \right) \frac{\partial k}{\partial x_j} \right] + P_k - \rho\varepsilon, \quad (7)$$

$$\frac{\partial(\rho\varepsilon)}{\partial t} + \frac{\partial}{\partial x_j} (U_j \rho\varepsilon) = \frac{\partial}{\partial x_j} \left[\left(\mu + \frac{\mu_t}{\sigma_{\varepsilon}} \right) \frac{\partial \varepsilon}{\partial x_j} \right] + (C_{\varepsilon 1} P_k - C_{\varepsilon 2} \rho\varepsilon + E) T_t^{-1}, \quad (8)$$

$$\mu_t = C_{\mu}^* f_{\mu} \rho k^2 / \varepsilon, \quad (9)$$

where $P_k = -\rho u_i u_j U_{i,j}$ is the exact turbulence production and the time scale is k/ε at large R_t , but becomes proportional to the Kolmogorov scale $(\nu/\varepsilon)^{1/2}$, for $R_t \ll 1$. The extra source term, E , is designed to increase the level of ε in non equilibrium flow regions

$$\psi = \max \left\{ \frac{\partial k}{\partial x_j} \frac{\partial \tau}{\partial x_j}, 0 \right\}, \quad (10)$$

$$\nu = \max \{ k^{1/2}, (\nu\varepsilon)^{1/4} \}, \quad (11)$$

$$E = A_E \rho \nu \sqrt{\varepsilon T_t} \psi, \quad (12)$$

where $\tau = \kappa/\epsilon$, is the turbulence time scale. The model constants are $C_{\epsilon 1}=1.44$, $C_{\epsilon 2}=1.92$, $\sigma_k=1.0$, $\sigma_\epsilon=1.0$, $A_\mu=0.01$ e $A_\epsilon=0.15$. The two transport equations are subjected to the following boundary conditions at solid walls,

$$k_w = 0, \tag{13}$$

$$\epsilon_w = 2\nu_t k_l / y_l^2, \tag{14}$$

where “1” denotes the centroid of the wall-adjacent cell and y_1 is the corresponding normal distance. The latter boundary condition is replaced by the Neumann condition $\epsilon\Omega = \epsilon 1$ when a wall function is invoked.

This model has been validated against various flow cases across the Mach number range. Details are given in the work of Goldberg et al. (2000) for hypersonic flows and in Goldberg et al. (1999) for subsonic, transonic and supersonic flows.

The governing equations are discretized and solved using the techniques embedded in the CFD++ package. Steady-state solutions are sought with the aid of a pre-conditioner which increases the convergence rate.

Table 1: Coefficients of the non linear terms.

a_1	a_2	a_3	b_1	b_2	b_3	b_4
$\frac{3 \cdot f_\mu}{1000 + S^3}$	$\frac{15 \cdot f_\mu}{1000 + S^3}$	$\frac{-19 \cdot f_\mu}{1000 + S^3}$	$-16 \cdot (C_\mu^*)^3 f_\mu$	$-16 \cdot (C_\mu^*)^3 f_\mu$	0	$80 \cdot (C_\mu^*)^3 f_\mu$

3. Computational Meshes Used

This section presents a study of the influence of different mesh configurations on the distribution of the pressure coefficient around the NLR7301 airfoil, and on the calculated value of the lift, drag and friction coefficients. Four different values for the AoA (angle of attack) 6.7° , 11.3° , 14.2° and 17.3° are considered, where the biggest one relates to an after stall situation in the tunnel tests.

All meshes used present a hybrid configuration, *i.e.*, they have two different cell types in its discretization: a quadrilaterals layer in the vicinity of the airfoil and triangles that span from this layer until the region of non disturbed flow far from the airfoil.

The aim of the quadrilaterals layer is to efficiently capture the viscous effects in the vicinity of the wall, *i.e.*, at the boundary layer, and it presents an uniform height, D , along the airfoil. The height of the first cell next to the wall, d , is also constant along the airfoil and both are calculated as follows:

$$d = 5.893 y^+ C Re^{-0.9}, \quad D = 0.37 C Re^{-0.2}, \tag{15}$$

where Re is the Reynolds number, C is a geometric scale, in this case the chord length ($C = 1m$), and y^+ is the classical non dimensional distance to the wall, which controls the height of the first cell and is here taken of order 1, as usual for low Reynolds numbers computations (Wilcox, 1993).

The tests analyzed here present Re of $2.85 \cdot 10^6$. The values of the parameters D and d chosen are $1.89cm$ and $4.68 \mu m$, respectively, which allow, according to Eq. (1), for a correct description of the boundary layer in the range 2.85 to $6.0 \cdot 10^6$. These geometric parameters are kept constant throughout the paper, regardless the number of mesh points used.

3.1. Mesh A

This mesh, shown in figures 1, is made of 573210 quadrilaterals and 290483 triangles. An abrupt transition exists from the quadrilaterals to the triangles, which is characterized by a change in the surface area of the computational cells of up to two orders of magnitude.

Note that, with the purpose of achieving a better control of the quality of the mesh a tool dubbed “capsule” was used. This tool creates a region around the airfoil, inside which the density of the computational cells is increased. The effect of this tool can be observed in figure 1. All capsules tested span from the leading-edge until 1.5 chord lengths downstream of the trailing-edge. The choice of the position of the capsule will be shown to be essential for the computations at high angle of attack. Indeed, for high values of AoA, a correct prediction of the flow at the suction side in the vicinity of the trailing

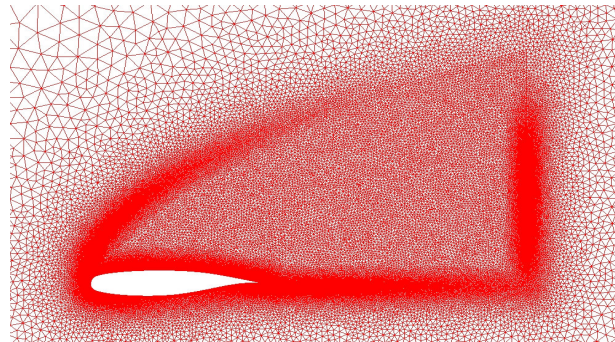


Figure 1: Mesh A around the airfoil and the capsule.

edge will be shown to be crucial for the determination of the maximum lift coefficient for this airfoil.

3.2. Mesh C

This is the only mesh for which the capsule is not used, as can be seen in figure 2. The number of quadrilaterals, distributed in the boundary layer, is about 336000 (less than mesh A) and the number of triangles 36267, an order of magnitude smaller than mesh A. Without the capsule it is hard to guarantee a good discretization and a smooth growth of the cell density when coming from the region of undisturbed flow and getting closer to the turbulent wake of the airfoil.

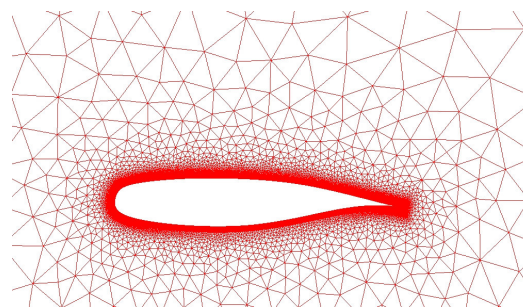


Figure 2: Mesh C around the airfoil.

3.3. Mesh D

This mesh, shown in figure 3, if not for the presence of the capsule, and the consequent larger density of the cells in the upper-side and in the region of turbulent wake, is very similar to mesh C. The region of boundary layer is exactly the same as for mesh C, with 336000 quadrilaterals, but the capsule used here leads to 87700 triangles.

A detailed exam of mesh D shows that some quality problems found in mesh A have been corrected. Some mismatches of cell surface areas still exist, albeit less than those of mesh A.

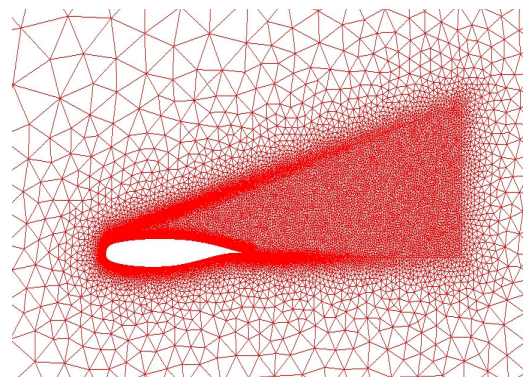


Figure 5: Mesh D around the airfoil.

4. Results and Discussion

The freestream conditions for the Mach number, Reynolds number and temperature used in the present computations are 0.201, $2.85 \cdot 10^6$ and 285K, respectively. The turbulence intensity and length scale are $T = 1.0 \cdot 10^{-2}$ and $L = 1.0 \cdot 10^{-3}$. These quantities are defined as $T = U_\infty^{-1} \sqrt{2k/3}$ and $L = (C_\mu k)^{3/2} / \kappa \mathcal{E}$, with $C_\mu=0.09$ and $\kappa=0.41$.

Initially it is investigated whether the numerical calculation convergence could be achieved for all AoA. The aerodynamic coefficients, particularly CL (lift coefficient) are compared to the tunnel tests results. The smallest angles of attack showed no convergence problems. However, when $\alpha = 17.3^\circ$, after stall in tunnel tests, convergence is not achieved. With the meshes C and D, the flow is simulated in the same condition as for mesh A, yet for only one AoA, the highest obtained with mesh A.

4.1. Computational results obtained with mesh A

The computations are performed for four values of angle of attack, 6.70° , 11.32° , 14.15° and 17.29° . For the first three values of AoA the evolution of the pressure coefficient (CP) along the surface of the airfoil obtained with mesh A is shown in figures 6 to 8. The corresponding values of the coefficients of lift, drag and momentum are given in Table 2, together with the measured values for these coefficients. In these figures, the largest discrepancies observed between computed and measured results are found in the suction peak and near the trailing edge. Except near the trailing edge,

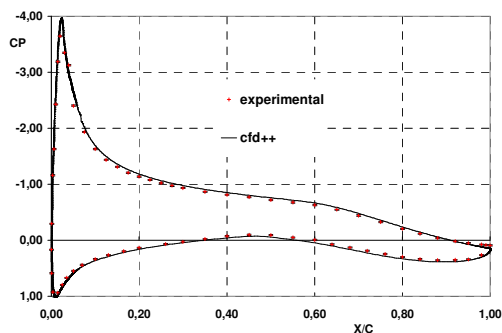


Figure 6: Pressure coefficient along the airfoil for $\alpha 6.70^\circ$, mesh A.

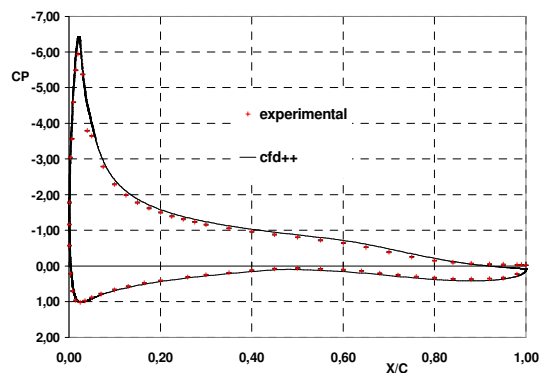


Figure 7: Pressure coefficient along the airfoil for $\alpha 11.32^\circ$, mesh A.

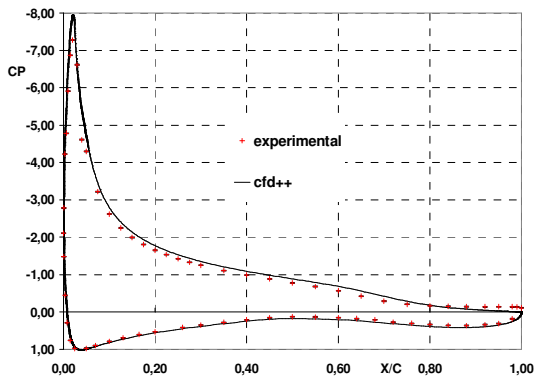


Figure 8: Pressure coefficient along the airfoil for alpha 14.15°, mesh A.

the computations under predict CP for the upper side, while the reverse is true for the lower side. The discrepancy at the upper side is larger than that at the lower side, what, in addition to the discrepancy at the suction peak, can explain the difference on the computed CL values, which higher than the tunnel values, as shown in Table 2. Concerning CL, the highest difference, +10.15%, was obtained for alpha equal to 14.15° and the lowest, for alpha 6.7°, was +8.5%.

For the drag coefficient, CD, it can be noted in Table 2 a discrepancy relative to the tunnel results considerably larger than that for CL. This discrepancy falls from 63% to 3.4%, when alpha is raised from 6.7° to 14.15°, respectively.

The computational results obtained for CL and CD show a similar behavior to other softwares used by the Computational Aerodynamics Group from Embraer (AAC), in numerical simulations with airfoils, wings and fuselages, subjected to different AoA (Drela, 1989, Drela and Giles, 1987). Particularly, the values calculated for CD at low AoA present a worst result than that calculated at high angles.

Table 2: Comparison between the tunnel tests and the present simulations results, mesh A.

test	CL	ΔCL	CD	ΔCD	CM_{25}	ΔCM_{25}
alpha 6,70 tunnel	0.964	-	0.0108	-	0.0638	-
CFD++	1.046	8.5%	0.0176	63.0%	0.0777	21.8%
alpha 11,32 tunnel	1.356	-	0.0250	-	0.0508	-
CFD++	1.489	9.8%	0.0291	16.4%	0.0675	32.9%
alpha 14,15 tunnel	1.531	-	0.0385	-	0.0394	-
CFD++	1.692	10.5%	0.0398	3.4%	0.0552	40.1%
alpha 17,29 tunnel	1.193	-	0.1296	-	0.0910	-
CFD++	-	-	-	-	-	-

The differences observed come, at least partially, from the fact that the coefficients CL and CD are calculated from the integration of the pressure and the viscous forces along the surface of the airfoil. Consequently, for low values of AoA, the number of cells over the airfoil in the direction perpendicular to the undisturbed flow, *i.e.*, the direction in which the drag force acts, is relatively small, if compared to the number of cells parallel to this direction, which is the lift direction. This small spatial resolution in the transverse direction may cause a considerable error in the determination of CD. As alpha is increased, the number of cells which contribute for the calculation of the drag also increases. Hence, this could explain the increased accuracy in the calculation of the drag when the AoA grows. Another possible cause for the observed discrepancy in the computed values of CD is the accurate prediction of laminar to turbulent transition. Indeed, the transition is free to occur both in the experiments and in the computations.

The values of the moment coefficient, CM, shown in Table 2, present a large discrepancy, ranging from 22% to 40%, when compared to the tunnel tests. This coefficient also comes from the integration of the CP value along the airfoil. Therefore, the even the small discrepancies observed for CP, which are situated far from the center of pressure,

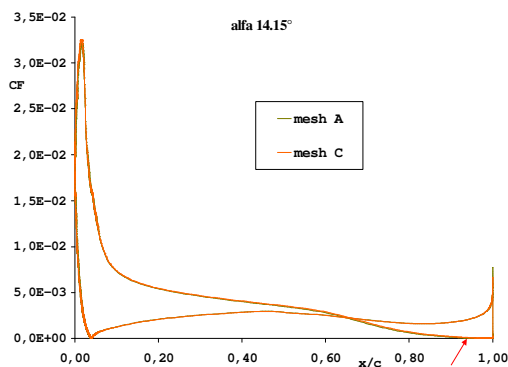


Figure 9: Comparison of the friction coefficient along the airfoil for meshes A and C, alpha=14.13°.

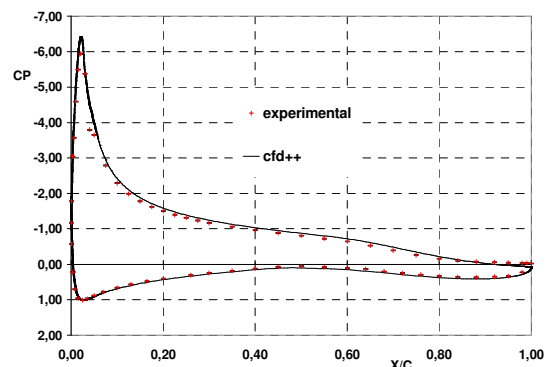


Figure 10: Pressure coefficient along the airfoil for alpha 11.32°, mesh A.

could influence the computed values of CM. This could explain the error in the determination of CM relative to the tunnel tests.

The curve for the friction coefficient obtained for alpha 14.1495° is given in figure 9. In this figure it can be observed, near the trailing edge, that the curve touches the horizontal axis, indicating that a slight separation of the flow seems to occur there.

The curve for Y+, given in figure 10, shows a behavior similar to CF, in particular, a slight separation near the trailing edge is noted. It should also be noted that the maximal value for Y+ is approximately 3 at the suction peak. Yet, for low Reynolds number turbulence models, as used here, it is recommended that the Y+ value be below 2. The value of Y+ above 2 in the vicinity of the suction peak can explain the discrepancies observed in the determination of CP and CM.

Table 3: Comparison of the values of the coefficients CL, CD and CM₂₅, obtained with the different meshes, for alpha equal to 14°.

test	CL	ΔCL	CD	ΔCD	CM ₂₅	ΔCM ₂₅
tunnel:	1,531	-	0,0385	-	0,0394	-
CFD++: mesh A	1,692	10,5%	0,0398	3,4%	0,0552	40,1%
mesh D	1,696	10,8%	0,0409	6,2%	0,0564	43,1%
mesh C	1,720	12,3%	0,0437	13,5%	0,0615	56,1%

4.2. Tests with different mesh configurations

Mesh A has about 850 000 cells. It was the finest mesh used in this work. Hence, the results obtained with mesh A served as parameter to evaluate the results computed with meshes C and D.

In Table 3, a comparison is presented between the results obtained with meshes A, C and D for AoA of 14.15°. It can be noted that the variation in relation to the wind tunnel value of CL is of 10.5%, for mesh A, which is the most refined one, to 12.3% for mesh C, which is the coarser one. As far as the drag coefficient is concerned, the discrepancy in relation to the tunnel value varies from 3.4% with mesh A to 13.5% with mesh C.

Figure 11 shows the evolution of the pressure coefficient along the chord for the different meshes used. In this figure it can be clearly seen that only slight differences are obtained between the three meshes and that all the results overestimate the suction peak.

In figure 12, in which are given, for the three meshes, the evolutions of CF in the vicinity of the trailing edge, it can be observed that the results obtained with meshes A and D are similar, while the values calculated for CF with mesh C are substantially higher. This discrepancy is probably due to the fact that the discretization of mesh C, downstream of the trailing edge, exhibits a more abrupt variation of cell size than meshes A and D. As a consequence of the rapid growth of the cells size, there is an increased dissipation of the flow variables in the turbulent wake downstream the airfoil. This point will be discussed be in the next section.

4.3. Tests with different mesh configurations

In Figs 13 to 15 a comparison is made of the effect of the different discretizations in the vicinity of the trailing edge on the calculated Mach number contours. In figure 14 it can be noted that the rapid growth of the mesh cells in mesh C is related to a strong dissipation of the wake downstream the trailing edge. On the contrary, the dissipation observed in figures 13 and 15, for meshes A and D, respectively, is not so strong and the discrepancy between both is hard to be noticed.

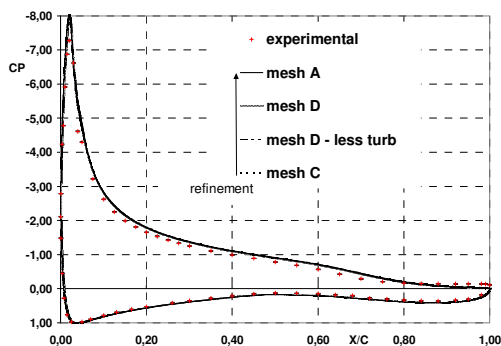


Figure 11: Pressure coefficient along the airfoil for different meshes, alpha 14.15°.

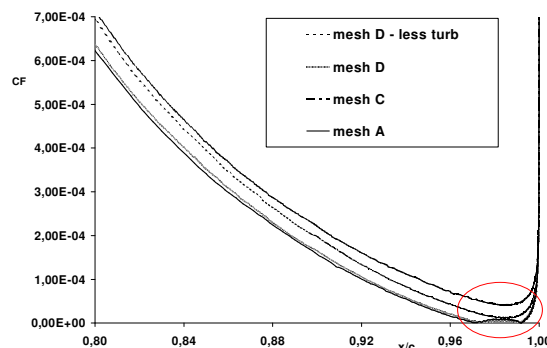


Figure 12: Friction coefficient on the suction side near the trailing edge. alpha 14.15°.

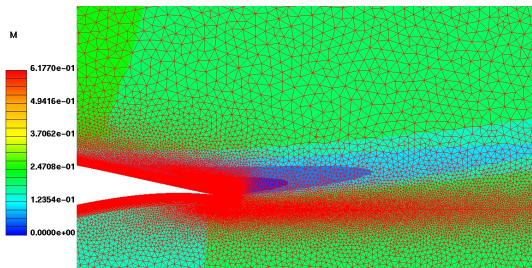


Figure 13: Mach number contours for mesh A.

These results confirm the importance of the capsule to guarantee a sufficient density of cells in the area external to the boundary layer, but still close to the airfoil, i.e., the region near the upper side and the trailing edge.

4.4. Obtaining the CL x Alpha Curve

In this section the lift curve as a function of the AoA (CL x ALPHA) is determined for the NLR7301 airfoil (Han, 1995), with the mesh that presented the best compromise between size and accuracy in the first part of the study, the mesh D. For this purpose, it is found necessary to adjust the turbulence parameters in order to guarantee the best agreement possible of the results from the wind tunnel.

The turbulence parameters used to obtain the initial CLxALPHA curve were turbulence intensity $T = 0.01$ and turbulence length $L = 0.001$, that leads to a turbulent to laminar viscosity ratio $\nu_t / \nu = 15.782$. Fourteen values of the AoA between 0° and 20.50° are then computed. The corresponding CLxALPHA curve is shown in figure 16. For the initial curve obtained, until AoA equals 16.05° the maximal error for CL is 11.95%. For higher values of the AoA the tunnel test presented considerable separation, with a corresponding decrease of the lift force (stall), while for the numerical calculation this only happens for alpha around 17° . Hence, for alpha above 16° the numerical results obtained have much larger discrepancies when compared to the tunnel results.

After the first CLxALPHA curve is obtained, one case, pre-stall in the tunnel tests (alpha 15.53°), is chosen in order to calibrate the turbulence parameters. The tunnel value for the turbulence intensity was not available, but, Ref. 4 states that its value is expected to be low “due to the characteristics of the tunnel”. Then, keeping the freestream turbulent intensity value constant, the value of the incoming turbulent length scale has been gradually increased from $L=0.001$ until 0.015, for which the CL value obtained equals the tunnel value. Using the freestream values obtained from this adjustment a corrected CLxALPHA curve is obtained for AoA varying between 0° and 19° . The result of this procedure is shown in figure 16.

Figure 17 shows the evolution of the pressure coefficient along the chord length when L is varied. The CP curve obtained when $L = 0.015$ is practically identical to the tunnel curve. An increase in the value of L causes the CL value to fall, from 1.76 (case 0) to 1.63 (case III), when L is varied from 0.001 to 0.015, respectively. Note that the tunnel CL value for this alpha (15.53°) is 1.59. Therefore, the result of case III is considered sufficiently close to the tunnel value, with an error margin of 2.5%.

After adjusting the turbulence parameter L, a second CLxALPHA curve was obtained, which presents a better agreement when compared to the tunnel tests. While the initial CLxALPHA curve could predict neither the CLmax, nor

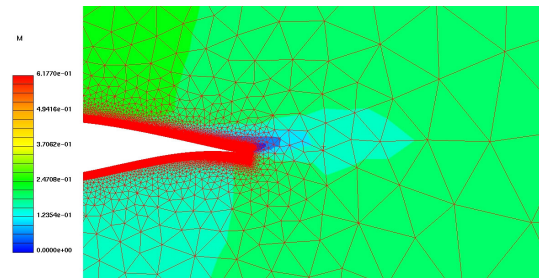


Figure 14: Mach number contours for mesh C.

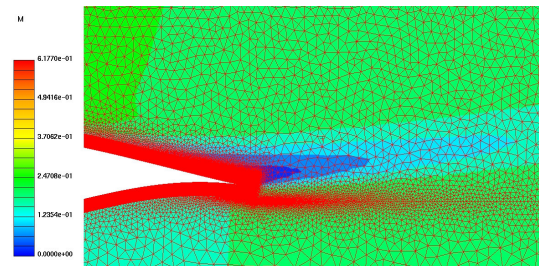


Figure 15: Mach number contours for mesh D.

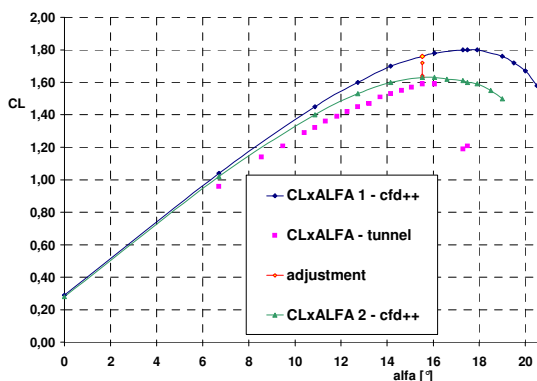


Figure 16: CLxALPHA curve – Comparison between the tunnel results and the present

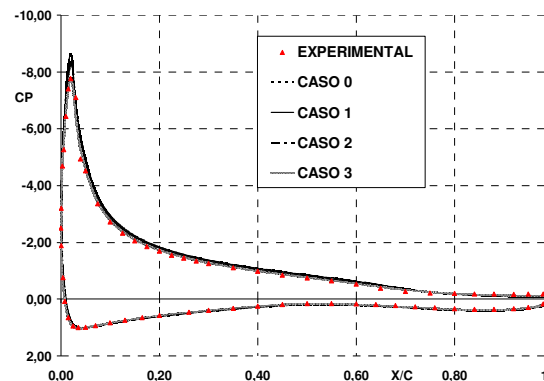


Figure 17: Pressure coefficient along the airfoil for different values of the turbulent length scale.

the ALPHAmax value, the adjusted curve, with an error margin of about 2.5%, obtained both values. Figure 19 presents the initial CLxALPHA curve, the adjusted one and the tunnel results. It should also be noted that the CLxALPHA curve, after the adjustment, presents a slope closer to the tunnel than the initial CLxALPHA curve.

Until alpha 16.05°, the maximal error for CL is 6.25%, for alpha 6.7°. Both the tunnel and the numerical result (after the adjustment) are coherent predicting a maximal value for the AoA, ALPHAmax=16.05°. However, the maximal CL value for the numerical calculation, CLmax =1.63 was 2.5% higher than the tunnel value, 1.59.

Despite this favorable result, the shape of the computed curve near the stall does not reproduce the tunnel result. For high AoA, the computed curve has a smooth fall, which is characteristic of the stall caused by a gradual propagation of the separation around the trailing edge toward the leading edge. Nevertheless, the stall observed in the tunnel tests seems to be abrupt, with a sudden fall of the CL value just after it reaches its maximal value. This behavior is typical of a leading edge stall, caused by the onset, development and collapse of a laminar separation bubble. However, tunnel results for a Reynolds number of $2.6 \cdot 10^6$ exhibit a gradual decrease of the CLxALFA curve, typical of the computed trailing edge stall.

In figure 18, the final CDxCL curve yields a better approximation to the tunnel results than after the adjustment. This is an outcome of the better representation of the lift coefficient. Even though the initial curve shows a small discrepancy until an AoA of 16°, the error diminishes for alpha values above this one.

In figure 19 the pitch moment coefficient is presented as a function of alpha (CMxALPHA), before and after the adjustment. It can be observed that, after the adjustment, the numerical curve is closer to the tunnel curve, and exhibits a similar behavior, yet displaced to higher alpha values. It is also interesting to note that the numerical results present an important discrepancy concerning the tunnel results for moderated alpha values.

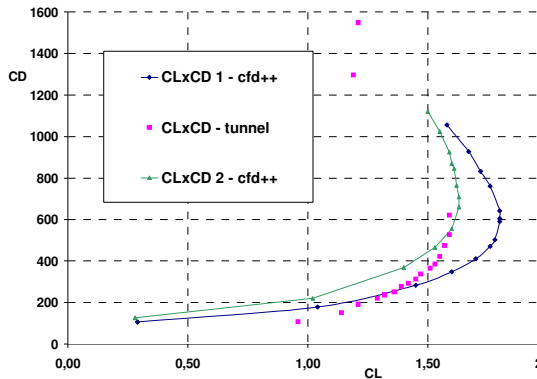


Figure 18: Drag polar curve.

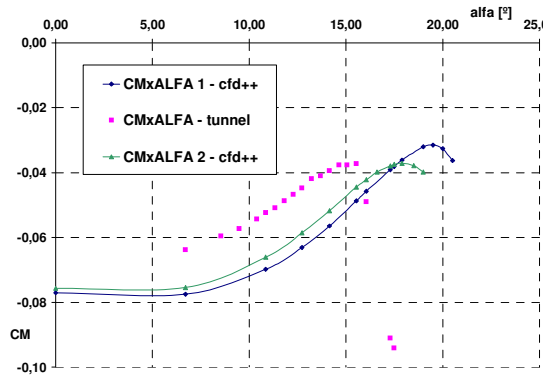


Figure 19: CMxALPHA curve.

5. Conclusions

Initially, a mesh sensitivity study of the flow around the NLR7301 airfoil was performed with the aim of obtaining mesh independent results for both the attached and the detached flow regimes. This required computational meshes with a large number of computational cells over the suction side of the airfoil and in the vicinity of the trailing edge. The influence of the freestream flow properties on the computed pressure distribution and on the lift and drag coefficients was assessed. In particular, the roles of the intensity of the turbulent fluctuations and of the averaged turbulence length scale were examined. The latter was shown to exert a strong influence on the aerodynamic coefficients of the airfoil, specifically in flow conditions near the aerodynamic stall.

Then, the lift coefficient curve was computed, and a good agreement was obtained between the calculated values of maximum lift coefficient and of the angle of attack where this value is observed. However, the post stall behavior of the computed solution is characteristic of a trailing edge stall, while the wind tunnel results exhibit an abrupt decrease of the lift coefficient after stall. This behavior is characteristic of the presence and subsequent coalescence of a laminar separation bubble at the suction side of the airfoil, which is probably absent from the computational results. Note, however, that for values of Reynolds number less than 10% larger than the one used in the present computations, wind tunnel results obtained for the same airfoil exhibit a completely different post-stall behavior. Indeed, there seems to exist a wind-tunnel dependence of the post-stall characteristics, indicating that the post-stall flow could not be considered as two-dimensional in the experiments.

The absence of the laminar separation bubble in the computed results could also explain the discrepancies observed in the drag coefficient curve. This bubble would lead to a higher drag, and thus to a lesser need in terms of the adjustment of turbulence length scales. Indeed, the corrected CD curve overpredicts the drag, whereas the curve initially calculated underpredicts the value of CD.

Concerning the pitching moment coefficient curve, although the overall behavior was correctly reproduced by the computations, discrepancies were observed on the actual value of this coefficient. These discrepancies may be attributed to small differences on the computed value of the distribution of pressure coefficient close to the leading and trailing edge. These differences in CP have a large contribution to the computed value of CM, due to their large distance to the moment reference point of the airfoil.

6. Acknowledgement

During this work L.F. Figueira da Silva was on leave from *Laboratoire de Combustion et de Détonique, Centre National de la Recherche Scientifique*, with a PROFIX scholarship from CNPq-Brazil.

7. References

- Drela, M., 1989, "XFOIL: An Analysis and Design System for Low Reynolds Number Airfoils," in *Low Reynolds Number Aerodynamics*, T.J. Mueller, editor. Lecture Notes in Engineering #54, Springer-Verlag.
- Drela, M. and Giles, M. B., 1987, "ISES: A Two Dimensional Viscous Aerodynamic Design and Analysis," in 25th AIAA Aerospace Sciences Meeting, AIAA Paper 87-0424.
- Han, S. O. T. H., 1995, "Two-Dimensional 16.5% Thick Supercritical Airfoil NLR 7301," AGARD Advisory Report n° 303 "A Selection of Experimental Tests Cases for the Validation of CFD codes" - vol. I – Advisory Group for Aerospace Research & Development.
- Hirschel, E. H., 1999, "Present and Future Aerodynamic Process Technologies at DASA Military Aircraft," ERCOFTAC Industrial Technology Topic Meeting.
- Jameson, A. , 1996, "The Present Status, Challenges and Future Developments in Computational Fluid Dynamics," *Progress and Challenges in CFD Methods and Algorithms*, AGARD-CP-578.
- Lien, F. S. and Leschziner, M. A., 1996, "Low Reynolds Number Eddy-Viscosity Modelling Based on Non-Linear Stress-Strain/Vorticity Relations," *Engineering Turbulence Modelling and Experiments 3*, edited by Rodi, W. and Bergeles, G., Elsevier, Amsterdam, pp. 91-100.
- Loyau, H., Batten, P. and Leschziner, M.A., 1998, "Modelling Shock/Boundary-Layer Interaction with Non-Linear Eddy-Viscosity Closures," *Flow, Turbulence and Combustion*, Vol. 60, No. 3, pp. 257-282.
- Goldberg, U., Batten, P., Palaniswamy, S., Chakravarthy, S. and Peroomian, O., 2000, "Hypersonic Flow Predictions Using Linear and Nonlinear Turbulence Closures," *Journal of Aircraft*, Vol. 37, No. 4, pp.671-675.
- Goldberg, U., Peroomian, O., Palaniswamy, S. and Chakravarthy, S., 1999, "Anisotropic k-ε Model for Adverse Pressure Gradient Flow," 37th AIAA Aerospace Sciences Meeting and Exhibit, AIAA Paper 99-0152.
- Palaniswamy, S., Goldberg, U., Peroomian, O. and Chakravarthy S., 2001, "Predictions of Axial and Transverse Injection into Supersonic Flow," *Flow, Turbulence and Combustion*, Vol. 66, No. 1, pp. 37-55.
- Peroomian, O. and Chakravarthy, S., 1997, "A 'Grid-Transparent' Methodology for CFD," 35th AIAA Aerospace Sciences Meeting and Exhibit, AIAA Paper No. 97-0724.
- Shih, T. H., Lumley, J. L. and Zhu, J., 1993, "A Realizable Reynolds Stress Algebraic Equation Model," NASA TM-105993.
- Vos, J. B., Rizzi, A., Darracq, D. and Hirschel, E. H., 2002, "Navier-Stokes Solvers in European Aircraft Design," *Progress in Aerospace Sciences*, Vol. 38, No. 8, pp. 601-69.
- Wilcox, D. C., 1993, "Turbulence Modeling for CFD," DCW Industries, 2nd edition.